Applications of hyperspectral mineralogy for geoenvironmental characterisation

N. Fox [a,*], A. Parbhakar-Fox [b], J. Moltzen [a,c], S. Feig [d], K. Goemann [d], J. Huntington [e]

a Discipline of Earth Sciences, University of Tasmania, Hobart, Tasmania 7001, Australia

b Transforming the Mining Value Chain, ARC Industrial Transformation Hub, University of Tasmania, Hobart, Tasmania 7001, Australia

c Mineral Resources Tasmania, Department of State Growth, Tasmania 7018, Australia

d Central Science Laboratory, University of Tasmania, Hobart, Tasmania 7001, Australia

e CSIRO Mineral Resources, PO Box 52, North Ryde, NSW 1670, Australia

Abstract

Technological innovations and emerging analytical capabilities are transforming the mineralogical and textural analysis of rock samples and drill core. Accurate mineralogical identification and systematic documentation can enhance deposit knowledge across the mining chain. From the earliest stages of mine-life, accurate mineralogical identification can also enhance environmental characterisation which traditionally utilises a range of wet chemical tests to predict acid generation and acid neutralisation potential. An enhanced understanding of both the ore and gangue mineralogy allows accurate prediction of the geoenvironmental characteristics of future waste materials. This study presents examples using thermal infrared (TIR) hyperspectral data for domaining acid neutralisation capacity in an exploration drill hole in a volcanic hosted massive sulfide (VHMS) district and a porphyry Cu-Au deposit by rapidly identifying the distribution and relative abundance of carbonate-group minerals. The results are validated using mineralogical and chemical analytical techniques (XRD and EMPA) and are compared to industry standard chemical tests (paste pH, NAG pH) used for acid base accounting (ABA) of mine materials. Utilising hyperspectral core scanning platforms for identifying acid neutralising domains can facilitate deposit-scale geoenvironmental modelling from the earliest of mine stages and improve long-term waste management practices.

1. Introduction

There is continuing demand for discoveries of large (>500 Mt) to giant (>1000 Mt) deposits of copper, gold, molybdenum and other metals to account for compound annual growth in metal demand of 2–3% per annum (Jennings and Schodde, 2016). Future mines must contain adequate resources (both grade and tonnage), provide long mine lives (>30 years) and be able to operate with low production and energy costs. Significantly, environmental and social responsibility is becoming increasingly important for the development of new mining operations. Environmental protection legislation and increased social awareness of the potential environmental risks associated with mining can impact the development of new mines.

Environmental prediction test work is typically carried out at the pre-feasibility and feasibility stages of mine development (GARD Guide, 2014). Field- and laboratory-based chemical tests and kinetic trials are used to determine acid rock drainage (ARD) formation potential of low or no grade material which has been designated as waste in block models and mine plans (White et al., 1999, Parbhakar-Fox and Lottermoser, 2015). However, these chemical tests are typically non-reproducible, costly and time consuming and therefore, may only be carried out on a restricted number of samples considered to be representative of larger intervals

of a particular rock unit or alteration type. Furthermore, traditionally the tests focus on wet chemical techniques with only minor consideration of mineralogical variability.

However, improved geoenvironmental assessments have been achieved by integrating process mineralogy tools such as automated mineral analysers including the MLA and QEMSCAN with traditional predictive chemical tests (Parbhakar-Fox et al., 2011, Brough et al., 2013, Parbhakar-Fox et al., 2013). However, the long analysis time and high cost of MLA (>$500 USD per sample) makes this a non-routine approach for characterising waste materials. Instead, we document the use of hyperspectral mineral analysis and core scanning technologies to map the distribution of acid neutralising domains in drill core and document how this can be used to reduce the subjectivity associated with sampling for chemical predictive environmental testing. Geoenvironmental risk assessments based on mineralogical mapping of drill core enables enhanced deposit-scale characterisation of waste rock domains and allows for more targeted static and kinetic testing for developing more accurate geoenvironmental risk models.

2. Hyperspectral mineralogical techniques

Hyperspectral reflectance spectrometers are widely used for mineralogical applications in airborne and satellite remote sensing applications including for mapping regional-to district-scale geological and alteration features (Laukamp et al., 2011, Yang et al., 2011, van Ruitenbeek et al., 2012) and more recently for mapping acid mine drainage (Ong and Cudahy, 2014). Field portable, non-automated hyperspectral reflectance spectrometers (e.g., PIMA, TerraSpec™) analysing the near infrared (NIR) to shortwave infrared (SWIR) wavelengths are capable of identifying phyllosilicates (mica, clay and chlorite), sulfates (alunite, gypsum and jarosite), carbonates (calcite, dolomite, ankerite and magnesite) and hydroxylated silicates (e.g., epidote and amphibole) based on diagnostic spectral absorption features (Yang et al., 2011, Laakso et al., 2016). Absorption features recorded in VNIR and SWIR reflectance spectra are mainly caused by sub-molecular vibrations (bending and stretching) of molecular bonds in response to the absorption of specific wavelengths of light. Mineral species produce characteristic absorption features which correspond to specific molecular bonds such as OH, H2O, CO3 and other components of hydrous silicate minerals including Alsingle bondOH, Mgsingle bondOH and Fesingle bondOH bonds (Fig. 1; Hunt and Salisbury, 1971, Hunt and Salisbury, 1973, Gaffey, 1986).

Anhydrous silicate minerals including quartz, feldspar-group and pyroxene-group minerals do not produce characteristic VNIR-SWIR reflectance spectra because they lack cations bonded to OH molecules. These mineral groups can be identified using dedicated spectrometers measuring in the thermal infrared (TIR) part of the electromagnetic spectrum (e.g., Huang and Kerr, 1960, Cudahy et al., 2009). Significantly, certain mineral groups, including carbonate-group minerals, which do produce spectral absorption features in the VNIR-SWIR region, also produce mineral specific reflectance spectra in the TIR region (Green and Schodlok, in press, Schodlok et al., in press). Combined VNIR-SWIR and TIR spectral analysis allows identification of a wide range of rock forming and alteration minerals for robust mineralogical mapping.

The first automated hyperspectral core scanner named the HyLogger was developed by the Commonwealth Scientific and Industrial Research Organisation (CSIRO) and acquired continuous downhole spectral mineralogy in drill cores (Huntington et al., 2011). The HyLogger-3 is equipped with VNIR, SWIR and TIR reflectance spectrometers which continuously analyse the drill core surface providing spectral data equivalent to spot measurements at 8 mm intervals (Mason and Huntington, 2012). Automated sample movement, spectral scanning and semi-automated data interpretation through dedicated software allows for rapid, continuous scanning of up to 1000 m of drill core per day (Mason and Huntington, 2012, Schodlok et al., in press).

Spectral imaging platforms, modified largely from airborne remote sensing applications, are now capable of producing 2D spectral images along the drill core surface. Systems include Corescan's HCI-3 platform(www.corescan.com.au) and SPECIM's SisuRock/SisuCHEMA system (www.specim.fi) which currently analyse in the VNIR-SWIR regions to generate spectral mineral maps with a spatial pixel resolution of approximately 0.5 mm. SPECIM's AISA OWL is a commercially available TIR hyperspectral imaging camera capable of mapping anhydrous minerals and carbonate-group minerals at a spatial pixel resolution of approximately 0.7 mm. The advantage of spectral imaging systems such as the SisuCHEMA/AISA OWL and Corescan platforms is the ability to integrate mineralogy with textural features including veins, vein envelopes and other rock textures (Huntington et al., 2010, Martini, 2013).

2.1. Carbonate mineralogy using hyperspectral techniques

Carbonate-group minerals produce distinctive spectral absorption features in the SWIR region, including the main diagnostic CO3 absorption feature located between 2300 and 2350 nm together with additional spectral features at 1870 nm, 1990 nm and 2155 nm (Fig. 1A; Gaffey, 1986). The specific position of the main 2300–2350 nm spectral feature (mean 2335 nm) for carbonates varies depending on carbonate mineral species with Mg-rich carbonates (e.g., magnesite) having a peak at shorter wavelengths (~2302 nm) compared to Ca-rich carbonates (e.g., calcite) at ~2340 nm (Fig. 1A, Table 1). The position of the 2335 nm spectral feature is commonly used for carbonate mineral identification in SWIR, particularly in routine or semi-automated processing platforms. Spectral overlaps in the 2335 nm region include the Mg-OH feature, typical of chlorite and a secondary Al-OH feature from muscovite and other white mica minerals (e.g., illite; Fig. 1A). Resolving carbonate mineralogy in mixed spectra which include muscovite and chlorite can be problematic in the SWIR region. A diagnostic feature for Fe-bearing carbonates occurs in the VNIR region at ~1200 nm related to crystal field absorption bands of Fe2+ ions (Gaffey, 1986, Green and Schodlok, in press). The gradient of this feature can provide distinction between Fe-bearing carbonates (e.g., siderite, Fe-dolomite, ankerite) and those with no Fe (e.g., calcite, magnesite). However, the carbonate diagnostics using this feature may also be compromised by other Fe-bearing phases (e.g., chlorite and biotite; Fig. 1A).

Spectral features for carbonate-group minerals in the TIR region occur at approximately 6,500 nm, 11,300 nm and 13,900 nm and the relative shifts in these spectral features can be used for carbonate-species diagnosis (Huang and Kerr, 1960, Lane and Christensen, 1997, Reig et al., 2002, Green and Schodlok, in press; Fig. 1B). Significantly, these TIR spectral features are not affected by spectral overlaps from chlorite or muscovite-group minerals (Fig. 1B) and offer advantages for carbonate mineral identification over VNIR-SWIR techniques alone.

3. Significance of carbonate-group minerals for environmental mineralogy

Acid rock drainage (ARD) is the generation of acidic, metal-rich waters caused by the oxidation of sulfide-bearing (e.g., pyrite, pyrrhotite) materials and represents a significant source of environmental risks at historical and active mine sites globally (e.g., Evangelou and Zhang, 1995, Dold, 2010). Acid generated in this may be neutralised by reaction with gangue minerals including carbonate-group minerals which represent the most significant primary neutralisers (Lapakko, 2002). Acid neutralising capacity (ANC) for pure carbonate minerals range between 374 and 1187 kg CaCO3/t for calcite (CaCO3) and dolomite (CaMg(CO3)2) providing the highest acid neutralising capacities (Jambor et al., 2007, Parbhakar-Fox and Lottermoser, 2015). Accurate identification of carbonate-group mineralogy has implications for robust calculation of the overall neutralising potential available in drill core materials, both in the ore and waste rock zones. Mineralogical tools including hyperspectral core scanning offer the potential to routinely delineate acid neutralising domains in drill core and build deposit-scale block models for improved waste and resource management. For this study, drill core samples containing a range of carbonate-group minerals were analysed in drill core from two deposit styles,

one a volcanic hosted massive sulfide (VHMS) prospect and one a porphyry Cu deposit. The aim was to test the classification of key carbonate-group minerals (including calcite, dolomite, siderite) using short wave infrared (SWIR) and long wave infrared (LWIR, or thermal infrared, TIR) hyperspectral techniques. Results were validated mineralogically using X-ray powder diffraction (XRPD) and electron microprobe analyses (EMPA) to test the accuracy of hyperspectral mineral identification with results compared to conventional chemical static tests (paste pH, NAG-pH) which are widely used for ARD prediction.

4. Deposit styles and study sites

Volcanic hosted massive sulfide deposits represent a class of typically low to medium tonnage (2–100 million tonnes), high-grade (1–15%) polymetallic resources of Cu, Zn, Pb, Au and Ag. They are characterised by highly sulfidic ores and waste rock which are typically dominated by pyrite, chalcopyrite, sphalerite and galena (Large, 1992). Because of their highly sulfidic nature and comparably relatively low acid neutralising capacity, VHMS deposits are recognised as one of the most potentially environmentally detrimental deposit-styles to mine (Taylor et al., 1995, Plumlee, 1999, Seal and Hammarstrom, 2003). In contrast, porphyry Cu-Au (-Mo) deposits typically represent high to very high tonnage (500 million tonnes to >1 billion tonnes), low grade (0.2–0.5% Cu, <0.4 g/t Au) resources amenable to a range of open pit and underground mining techniques (John et al., 2010). The ore mineralogy typically comprises bornite, chalcopyrite and molybdenite with broad zones of pyrite-rich alteration forming a halo around the mineralised system (Seedorff et al., 2005, John et al., 2010, Sillitoe, 2010). The acid neutralising behaviour of porphyry deposits depends largely on the composition of the host rocks (volcanic, intrusive, or meta/sedimentary e.g., quartzite) and the relative abundance of carbonate-group minerals introduced during alteration and mineralisation (Berger et al., 2008). Mineralised veins and associated alteration commonly contain carbonate (calcite or ankerite) with more distal propylitic alteration also containing carbonate-group minerals (Seedorff et al., 2005, Sillitoe, 2010). Significantly, shallow alteration in calc-alkaline porphyry systems typically comprises large blankets (several km2) of phyllic, argillic and advanced argillic alteration (Sillitoe, 2010) which is dominated by clay, muscovite and pyrite with a high net acid generating potential and low acid neutralising capacity (Plumlee, 1999).

4.1. Volcanic hosted massive sulfide (VHMS) mineralisation, Mount Lyell, Tasmania

The Mount Lyell mineral field, located in Western Tasmania, Australia (Fig. 2) has been in near-continuous operation since its discovery in 1893. The field contains more than 20 individual ore bodies and ore lenses and has historically produced over 1.2 million tonnes (Mt) of copper and 45 tonnes of gold (Corbett et al., 2014) with combined proven and probable reserves (as of March, 2010) of 9.5 Mt at 1.25% Cu, 0.3 g/t Au and 3.0 g/t Ag (www.cmt.com.au). The Mount Lyell mineral field occurs in the Mount Read Volcanics, a Cambrian sequence of sub-marine, felsic to intermediate (rhyolite to andesite) volcanics and sedimentary rocks which also host economic VHMS mineralisation at Rosebery, Hercules, Que River and Henty (e.g., Corbett et al., 2014 and references therein). The Mount Lyell Field (Fig. 2) is 6 km long by 3 km wide and hosts a range of mineralisation styles including disseminated pyrite-chalcopyrite (e.g., Prince Lyell), bornite-chalcopyrite (e.g., North Lyell), massive pyrite-chalcopyrite (e.g., The Blow or Iron Blow) and stratiform massive pyrite-galena-sphalerite ore bodies (e.g., Tasman Crown; Fig. 1; Walshe and Solomon, 1981, Huston and Kamprad, 2001). This pilot study uses one exploration drill hole (GLD001) from the Glen Lyell prospect located in the southwest part of the district (Fig. 1). Lithologically, this drill hole is dominated by a sericite-pyrite-chlorite altered unit termed the Lyell Schist (Fig. 2) which forms part of the core alteration zone within the district and hosts the majority of the copper ore lenses in the Mount Lyell field (Corbett et al., 2014). Carbonate alteration occurs mainly as disseminations and vug infill in the alteration halo of individual lenses at Mount Lyell (Large et al., 2001; Corbett et al., 2014).

4.2. Mount Polley, porphyry Cu-Au deposit, British Columbia

The Mount Polley district is located in British Columbia, Canada and comprises a cluster of alkalic porphyry Cu-Au-Ag deposits (Fig. 3). The district includes mined-out open cut mines, active open cut operations and numerous advanced exploration prospects with current reserves of 40.5 Mt at 0.32% Cu, 0.28 g/t Au and 0.6 g/t Ag (Imperial Metals, 2014). The Mount Polley district is hosted by silica undersaturated alkalic monzonite intrusions and breccias of the Mount Polley complex which has intruded the Nicola Group comprising basalt, andesite and minor limestone (Logan and Mihalynuk, 2005). This study focuses on a drill hole located in the Northeast Zone at Mount Polley, which was discovered by near-mine exploration in 2003 (Imperial Metals, 2014). The Northeast Zone is characterised by bornite-chalcopyrite rich ore zones with only a relatively minor abundance of pyrite (<1%) forming a peripheral zone (Fig. 3; Pass et al., 2014). Hydrothermal alteration assemblages at the Northeast Zone are carbonate-rich, a common feature of alkalic porphyry deposits, which have an alteration zonation that differs to classical calc-alkaline porphyry Cu-Mo-Au deposits (Lang et al., 1995, Holliday and Cooke, 2007).

5. Materials and analytical methods

5.1. Sample materials

The entire length of drill hole GLD001 (end-of-hole at 998 m) from the Glen Lyell prospect was analysed on the CSIRO HyLogger-3 (see below) before being visually logged for lithology and alteration features. Thirteen representative half-core samples were selected for further textural and mineralogical testing from GLD001 for this study. A complete continuous drill core from the Northeast Zone at Mount Polley was not available for this study however, 35 half-core samples from a single drill hole (WB04-26) were systematically arranged in order of increasing depth in a black (non-SWIR responsive) drill core box for hyperspectral mineral analysis using the HyLogger-3. A subset of 12 samples was selected for further mineralogical analysis including XRPD and static testing.

5.2. CSIRO HyLogger-3

Hyperspectral mineralogy was determined using the CSIRO HyLogger-3 located at Mineral Resources Tasmania, Mornington, Tasmania, Australia. Prior to analysis, all samples were allowed to dry completely and where necessary, cleaned thoroughly with a vacuum cleaner to ensure analysed surfaces were free of dust and other loose material. The HyLogger-3 comprises a high resolution (0.065 mm per pixel) digital line scan camera and a laser profilometer for measuring core height and core fractures at 0.2 mm resolution (Mason and Huntington, 2012). Drill core is moved automatically (x, y coordinates) using a robotic table. The instrument is equipped with three coupled spectrometers analysing the visible near-infrared (VNIR) region (380–1072 nm), the shortwave (SWIR) infrared region (1072–2500 nm) and the thermal infrared (TIR) region (6000–14,500 nm). Each spectrometer measures 12 spectra per second, equivalent to one spectrum every 4 mm of core length at a core movement speed of 48 mm/s. Considering overlapping of adjacent spectra, this equates to an overall spatial resolution for the spectral measurements of approximately 8–12 mm (Huntington et al., 2010, Mason and Huntington, 2012). The various data streams (digital imagery, laser profilometer data and spectral data) are compiled in a dedicated software package called 'The Spectral Geologist or TSG' (http://www.thespectralgeologist.com/). Radiance measurements recorded by the VNIR-SWIR spectrometers are converted to absolute reflectance using dark and white reference spectra measured on a closed-shutter and a white Teflon standard reference respectively. The TIR radiance data is converted to reflectance by first calibrating spectra to blackbody and gold-standard reference materials and performing ambient temperature corrections (Mason and Huntington, 2012). Parts of the drill core tray, drill core markers and other non-geological features are masked out in TSG leaving only spectrally responsive data.

The spectral resolution of the Hylogger-3 ranges from 4 nm in the VNIR-SWIR region between 380 nm and 1600 nm to 10 nm at 2500 nm (Schodlok et al., in press) but are resampled to 4 nm for analysis. The TIR

spectral resolution increases with longer wavelengths from 25 nm at 6000 nm to 120 nm at 14,500 nm giving an overall total of 873 spectral channels across the VNIR-SWIR-TIR range (Schodlok et al., in press).

5.3. X-ray powder diffraction (XRPD)

X-ray diffraction analysis of powdered samples (XRPD) was carried out using a Bruker D2 Phaser X-ray diffractometer located at the University of Tasmania. The instrument used an operating voltage of 30 kV and 10 mA and a cobalt X-ray tube to generate CoKα radiation with a wavelength of 1.79026 Å. A 0.6 mm (0.3°) fixed divergence slit, 2.5° soller slit and an Fe-filter were used. Each scan ranged from 5 to 90° (2θ) with a 0.02° step size and a measurement time of 0.6 s per step. Mineral phases were identified using Bruker DIFFRAC.EVA software package with the PDF-2 (2012 release) powder diffraction file mineral database. Semi-quantitative modal mineralogy was calculated using Bruker Topas software version 4.2 for Rietveld refinement using mineral structures from the PDF-2 (2012) resource. Typical limits of detection for this technique are between 0.5 and 1.0 wt.% modal abundance.

5.4. Static geochemical testing

Geochemical risk classification of representative samples from each deposit was carried out at the University of Tasmania. These included the paste pH testing and net acid generation (NAG) pH testing of powdered rock material. Paste pH testing followed the AMIRA P387A Handbook method (Smart et al., 2002) and was performed on 13 samples from Glen Lyell and 12 samples from Mount Polley. 20 ml of deionised water was added to 10 g of <75 µm powdered rock material, and the slurry was left to react for 16 h before measuring the pH values using a Mettler Toledo S47 SevenMulti™ dual pH/conductivity meter which was calibrated prior to use with pH 4 and pH 7 buffer solutions. The pH value of each sample was measured in triplicate, with the standard deviation calculated to be <0.5 pH units. In addition, net acid generation (NAG) pH testing was conducted following the method of Smart et al. (2002). Visual assessments of the drill core materials showed them to contain trace sulfide contents (<1 wt.%), therefore the single addition NAG test was decided to be most appropriate for use (Smart et al., 2002, Parbhakar-Fox et al., 2011). This test involves the addition of hydrogen peroxide (H2O2; 15%) in one 250 ml increment to 2.5 g of powdered rock material (<75 µm). The ARD risk potential was classified using a combination of paste pH, NAG pH and net acid producing potential (NAPP) calculations based on total sulfur and carbon values.

5.5. Total carbon and sulfur analysis

Total carbon and sulfur analyses were measured on powdered samples using an Eltra CS-2000 analyser located at the University of Tasmania, Australia. Between 200 and 300 mg of powdered sample was weighed into a ceramic crucible before being combusted at 1100 °C in a stream of pure (99.99%) oxygen. The resulting gas was analysed using four solid state infrared absorption cells. The instrument is calibrated using international standard reference materials with accuracy and reproducibility better than 0.04 wt.% for total C and 0.02 wt.% for total S. Total carbon and sulfur allow a conservative calculation to be made for the maximum potential acidity (MPA) and neutralising potential (NP) of a sample following stoichiometric calculations summarised in Parbhakar-Fox and Lottermoser (2015).

5.6. Electron microprobe analysis (EMPA)

Quantitative chemical analyses of carbonate minerals were carried out using a Cameca SX100 electron microprobe located at the Central Science Laboratory, University of Tasmania. Carbon coated samples were analysed at 15 kV and 10 nA with a beam diameter of 10 µm. Quantitative measurements were carried out by wavelength dispersive X-ray spectrometry on 5 WDS analysing crystals. Measurements were calibrated on

natural standard reference materials calcite (Ca), periclase (Mg), hematite (Fe), rhodonite (Mn), wollastonite (Si), jadeite (Na), orthoclase (K), barite (Ba), celestite (Sr, S), and gahnite (Zn). Oxygen was calculated by cation stoichiometry and carbon by stoichiometry to oxygen. Data was corrected for x-ray spectral interferences (e.g., Mn on Fe) using Probe for EMPA software developed by Probe Software Inc. Dolomite (Oberdorf Austria, Harvard 105064) was analysed as secondary standard.

6. Results

6.1. Visual mineralogical logging

Mount Lyell VHMS district - drill hole GLD001

Initial visual logging of drill hole GLD001 identified five distinct intervals or domains containing abundant veins and/or replacements dominated by soft (<4, Mohs scale), white to pale brown and pink minerals (Fig. 4). Based on the absence of reaction with cold dilute hydrochloric acid (the field test for calcite), the field interpretation for these minerals was ankerite, siderite or dolomite. These domains are separated by large intervals (10–100 s of metres) of grey to black, weakly-foliated chloritic schist with local quartz veins and disseminated pyrite, but with little to no visible carbonate minerals (Fig. 4C). These intervals were given a domain name 'host rock'.

Mount Polley porphyry Cu-Au deposit

Drill core samples from a single diamond drill hole (WB04-26) from the Mount Polley Mine were arranged in drill core boxes according to increasing depth to approximate a continuous drill core. The samples were logged using conventional visual logging techniques for lithology, alteration mineralogy and mineral texture. The samples are dominated by brecciated porphyritic monzonite which is cemented with, and overprinted by, veins of a soft white mineral (Fig. 5) that reacted with cold dilute hydrochloric acid. Based on these hand specimen characteristics, the field interpretation for the breccia cement and veins was calcite. The near ubiquitous occurrence of carbonate minerals throughout the drill hole meant that unlike at Glen Lyell, spatial carbonate-rich domains were not segregated visually at Mount Polley.

6.2. Carbonate mineralogy using TIR spectral features

Carbonate mineral identification here focusses on the TIR spectral features analysed by the HyLogger-3. Carbonate spectral features in the VNIR-SWIR regions were found to be compromised by spectral mixtures of carbonate minerals with chlorite and muscovite (Fig. 1). The TIR spectral features of reference library carbonate-group minerals have been presented by Green and Schodlok (in press). Binary plots of the 13,900 vs. 11,300 nm and the 11,300 vs. 6500 nm spectral features (Fig. 6) allow comparison of acquired spectra from the HyLogger-3 from unknown samples to reference library end-member compositions (e.g., calcite, dolomite, ankerite, siderite etc.). Automated spectral feature extraction macros (known as scalars) defined by Green and Schodlok (in press) for carbonate-group minerals were applied to all downhole spectral analyses from Glen Lyell and Mount Polley using The Spectral Geologist (TSG) software. The exported spectral features at 6500, 11,300 and 13,900 nm were then filtered using the criteria of Green and Schodlok (in press) to remove highly mixed spectra where the position of carbonate spectral features are modified by the presence of other minerals including albite and orthoclase.

6.2.1. Glen Lyell TIR carbonate mineralogy

Classification from all downhole analysis in GLD001 indicates the presence of two main carbonate-groups, siderite and ankerite/Fe-dolomite (Fig. 6A and B). Classification of the siderite-group using the 13,900 and 11,300 nm features (Fig. 6A) is due to the shifts in the 13,900 nm feature to shorter wavelengths (13,400–

13,500 nm) and the 11,300 nm to longer wavelengths (11,350–11,500 nm) compared to the ankerite/Fe-dolomite group. Distinction between Fe-dolomite and ankerite is based on a cut-off in the 11,300 nm spectral feature around 11,250 nm (Fig. 6A). This classification is consistent with the 11,300 vs. 6,500 nm discrimination plot (Fig. 6B) which again highlights the shift of the siderite 11,300 nm spectral feature to longer wavelengths compared to ankerite/Fe-dolomite and suggest a possible compositional solid solution towards rhodochrosite. Significantly, the results of this spectral analysis highlight the absence of calcite or dolomite in the entire drill hole at Glen Lyell. Each classified spectral analysis from Fig. 6A and B was plotted as a downhole histogram showing the number of counts for each mineral class (siderite, ankerite, Fe-dolomite) in 5 m bin intervals (Fig. 7). This highlights that the domains 1 and 2 in the shallow part of the drill hole (<330 m) contain both ankerite and siderite with a relative abundance of ankerite greater than siderite, based on counts (Fig. 7). Domain 3 located between 540 and 550 m contains siderite only and domain 4 contains both ankerite and siderite (Fig. 7). The deepest domain, domain 5 between 880 and 950 m has the highest relative abundance of carbonate (>400 counts) and is dominated by ankerite with lesser siderite and the only occurrence of Fe-dolomite (Fig. 7).

6.2.2. Other spectral features – barite

Barite (BaSO4) is a common accessory mineral in a range of hydrothermal ore forming systems but particularly the VHMS systems of Western Tasmania (Large, 1992). In hand specimen, it is commonly distinguished by its high specific gravity (4.5) but has a similar colour and hardness to carbonate-group minerals. Identification of barite and other sulfate minerals is important because ABA calculations using total sulfur determinations alone assume all sulfur in a sample to be due to the presence of sulfide minerals. A distinctive spectral feature for barite occurs at 10,100 nm in the TIR region making it possible to rapidly map the distribution of barite within drill cores using a similar feature extraction technique to that used for the carbonate-group minerals (Fig. 7).

6.2.3. Mount Polley TIR carbonate mineralogy

Processing of the Mount Polley drill core samples using the carbonate-group classification scalars indicates a bimodal distribution of the spectral data in the 13,900 vs. 11,300 nm plot (Fig. 6C) and a spread of data between kutnahorite and siderite in the 11,300 vs. 6500 nm plot (Fig. 6D). Each spectral analyses was individually examined using TSG and compared to reference library spectra. All the spectra from Mount Polley had a good spectral match for calcite, indicating that variation in the position of the 13,900 and 11,300 spectral features was likely caused by influence of coexisting minerals. Spectra that had a high spectral match for calcite with low degrees of spectral mixing were classified as ‘Calcite High” whereas those with a good spectral match for calcite but showed spectral mixing due to the presence of other minerals (e.g., albite, orthoclase) were labelled ‘Calcite Moderate’ (Fig. 6C and D). The filtering criteria of Green and Schodlok (in press) that filters out mixed spectra was relaxed for the 13,900 vs. 11,300 nm classification to show a downhole distribution of calcite from both the ‘Calcite High’ and ‘Calcite moderate’ classifications (Fig. 8).

6.3. Mineralogical validation

Bulk mineralogical (e.g., XRPD) and mineral specific (EMPA) techniques were used to verify the mineralogical classification of carbonate-group minerals determined by the TIR spectral technique. Drill core samples were selected from each main carbonate-bearing domain (domains 1–5) and host rock intervals at Glen Lyell (Fig. 8; Table 2) and from representative intervals at Mount Polley (Fig. 9; Table 3).

6.3.1. X-ray powder diffraction (XRPD)

6.3.1.1. Glen Lyell

X-ray powder diffraction and quantitative Rietveld refinement identified ankerite in the shallow domains 1 and 2 ranges between 7.3 and 21.8 wt.% which is higher in modal abundance than siderite which is typically below the limit of detection (<0.5 wt.%; Table 2; Fig. 8). The abundance of siderite in domains 3 and 4 is higher than ankerite (Table 2) which is consistent with the carbonate classification and relative abundance from TIR spectra (Fig. 8). Samples selected from domain 5 were only sampled from the siderite-dominant part of this interval which contains no detectable ankerite and is consistent with the spectral classification and relative carbonate intensity (Fig. 8). Diffraction peaks indicative of dolomite were not identified by XRD suggesting either the absence of dolomite (or Fe-dolomite) or a modal abundance that is below the limit of detection of XRPD (~0.5 wt.%). The drill core below 900 m depth was unavailable at the time of sampling. Consequently the mineralogy of deeper part of the drill hole was not verified by additional mineralogical techniques. Barite was measured by XRPD in the host rock domain at 288.1 m (10.1 wt.%; Table 2) and is consistent with the spectral identification of barite (Fig. 8). XRPD indicated that the host rock domains contain low carbonate contents (<0.5 wt.% total) with high pyrite contents only in the deeper host rock domain at 353.3 m (5.6 wt.%).

6.3.1.2. Mount Polley

XRPD indicated that samples analysed from Mount Polley contain only calcite with no other carbonate-group minerals detected (Table 3; Fig. 9). This verifies that the spread in the data points on the 13,900 vs. 11,300 nm discrimination diagram (Fig. 6C) is due to spectral interference of the diagnostic carbonate spectral features with coexisting minerals (albite, orthoclase) which XRPD shows to be present (Table 3).

6.3.2. Electron microprobe analysis

Results of the electron microprobe analyses of carbonate minerals from Glen Lyell and Mount Polley are shown on compositional diagrams in Fig. 9. Carbonate from Glen Lyell has complex chemical variability related to solid solutions between ankerite (Ca(Fe,Mg,Mn)(CO3)2) and dolomite (CaMg(CO3)2) and between siderite (FeCO3) and rhodochrosite (MnCO3). Carbonate from domain 1 is dominantly intermediate in composition between ankerite and dolomite (Fig. 9A and B) with minor manganiferous siderite (Fig. 9B and C) which is consistent with both the spectral classification and XRPD results. Domain 2 contains only carbonate intermediate in composition between ankerite and dolomite with only minor Fe and Mn (0.1 mol%; Fig. 9). Siderite with variable Mn and Fe concentrations was identified in domains 3 and 5 whereas a domain 4 contains both siderite and intermediate dolomite-ankerite (Fig. 9). Minor carbonate in the host-rock domains was confirmed to be similar in composition to the ankerite-dolomite in domains 1, 2 and 4 (Fig. 9) All samples from Mount Polley indicate that calcite is the only carbonate-group mineral present with only trace content of Mn in these carbonates (Fig. 9A and B). These results support the spectral carbonate identification and XRPD results.

6.4. Static testing and geoenvironmental classification

Static test results for Glen Lyell and Mount Polley are shown in Table 2, Table 3, respectively and illustrated in classification diagrams in Fig. 10. Calculated Net Acid Producing Potential (NAPP) indicates that host rock samples at Glen Lyell are potentially acid forming (PAF) whereas samples from all other domains are classified as non-acid forming (NAF; Fig. 10A). These classifications are confirmed in the paste pH vs. NAG pH plot (Fig. 10B). Significantly, the maximum potential acidity (MPA) of the host rock sample at 288.1 m has been overestimated due to the presence of barite (BaSO4) which was identified both spectrally (Fig. 7) and by XRPD (Table 2). All other samples from the carbonate-bearing domains were classified as non-acid forming, with negative net acid producing potential (NAPP; Fig. 10A). Variation in the NAPP values for Mount Polley samples (Fig. 10A) is caused by the variable proportions of calcite and pyrite/chalcopyrite (Table 3). Samples with overall carbonate to pyrite ratios >3:1 are classified as non-acid forming (NAF; Fig. 10A and B) and provide acid neutralising capacity (ANC; Parbhakar-Fox et al., 2011).

7. Discussion

7.1. Carbonate-group mineral identification using hyperspectral techniques

Drill core samples from Glen Lyell and Mount Polley contained a diverse range of carbonate-group minerals and provided an opportunity to evaluate the application of TIR spectral features for routine mineralogical domaining in drill core. The three main spectral features in the TIR region (6500, 11,300 and 13,900 nm; Green and Schodlok, in press) accurately identify siderite- and ankerite-group carbonates at Glen Lyell and calcite at Mount Polley (Fig. 7, Fig. 8). The spectral classification of Fe-dolomite at the base of GLD001 (Fig. 7) can be explained by the wide compositional solid solution between ankerite and dolomite determined by EMPA (Fig. 9). The TIR spectral features reflect progressive compositional variation of Ca, Mg, Fe and Mn in the carbonates and therefore, classification of Fe-dolomite may represent the most Mg-Fe rich carbonates analysed. Phase identification and quantification typically relies on reference libraries for end-member mineral compositions. Additional refinement of reference libraries for both spectral features and XRPD to include solid solution compositions (e.g., intermediate ankerite-dolomite compositions) will lead to improved mineralogical identification and quantification. Further advancements in quantifying the relative carbonate intensity or modal carbonate abundance from spectral data are intrinsic to the application of mineral domaining using spectral techniques.

The influence of spectral mixtures between carbonate, chlorite and muscovite is a limitation of VNIR-SWIR only spectra for accurate identification of the wide range of carbonate end-members (Fig. 1). However, TIR analysis as demonstrated here, offers improved diagnostics for carbonate-group mineral identification due to the presence of at least three spectral features which vary in position according to the chemistry of the carbonate minerals (Huang and Kerr, 1960, Reig et al., 2002, Green and Schodlok, in press). Whilst this study also identified spectral interferences between feldspar and calcite in the TIR at Mount Polley, the accurate identification of siderite and ankerite has significant implications for geoenvironmental domaining.

7.2. Geoenvironmental significance of mineralogical domaining

Accurate mineralogical identification is significant at all stages of the mine cycle from alteration mapping during exploration, resource drilling and deposit modelling to geometallurgical testing and prediction of geoenvironmental risks. Carbonate-group minerals are the most significant primary neutralisers of acid mine drainage (AMD) and understanding their distribution and abundance in an ore deposit has impacts for long-term mine waste management.

The neutralising capacity of waste materials are influenced by both the abundance and type of carbonate minerals present (Parbhakar-Fox and Lottermoser, 2015). The variability in neutralisation potential (NP) for individual carbonate minerals (Table 1; Jambor et al., 2007) and difference in dissolution rates means that carbonate mineral identification and quantification is imperative for accurate geoenvironmental domaining. Mineralogical determinations using XRPD and EMPA are impractical for routine analysis of drill core materials due to cost and time restrictions. Additionally, static geochemical testing, the industry standard practice for geoenvironmental characterisation, is not always accurate in predicting long-term geochemical behaviour of mine wastes, particularly in mineralogically complex systems (White et al., 1999, Parbhakar-Fox and Lottermoser, 2015, Dold, 2017).

The application of densely-sampled spectral techniques for identification of carbonate minerals used in this study has defined carbonate-bearing domains at the Glen Lyell VHMS prospect and at the Mount Polley

porphyry Cu deposit. The identification of ankerite-dolomite and siderite as the main carbonate minerals at Glen Lyell (Fig. 7) is reflected by the static geochemical testing which identified these domains to have low net acid producing potential (NAPP) and classifying them as non-acid forming (NAF; Fig. 10A and B). However, the effective neutralising capacity of domains 3, 4 and 5 which contain siderite may be overestimated because siderite can in fact produce acid through liberation of Fe^{2+} after its initial dissolution (Dold, 2017). Chemical testing is often used for siderite determinations (eg., ABCC testing; Smart et al., 2002) however, this is a costly and time consuming test which is rarely carried out routinely.

The incorrect estimation of maximum potential acidity (MPA) based on total sulfur data alone (Parbhakar-Fox and Lottermoser, 2015) is a significant source of error in ARD prediction (Downing and Giroux, 1993, Borden, 2003). Overestimation of the MPA can occur due to the presence of sulfate minerals which are incorporated into this calculation when based on total sulfur alone (Dold, 2017). The spectral data presented here identified a barite ($BaSO_4$) bearing domain at Glen Lyell (288.1 m) which contained low pyrite (<0.5 wt.%) but produced high MPA (Table 2; Fig. 10). This mineralogical information was used to indicate that the MPA was considerably overestimated by this calculation method. Mineralogical screening using the HyLogger-3 can identify sulfate minerals (barite, gypsum, alunite) to guide sampling and testing strategies to analyse for both sulfide- and sulfate-sulfur or to undertake modified Sobek testing (Dold, 2017). The absence of spectral responses for sulfate minerals from the HyLogger can give confidence to MPA calculations where total sulfur can be assumed to be from sulfide minerals alone. At Mount Polley, the absence of sulfate minerals detected in the spectral data and validated by XRD indicate the MPA calculations from total-sulfur represent contribution from the sulfide species (bornite, chalcopyrite and pyrite; Table 3).

The cost of AMD mitigation and control must be accurately predicted to reduce economic risks associated with environmental non-compliance during operations and after mine closure. Identification of neutralising domains at the deposit-scale has implications for long-term mine planning and management including design and construction of non-acid forming (NAF) waste dumps by blending potentially acid forming (PAF) materials with those with acid neutralisation capacity (ANC; e.g., Ok Tedi, PNG; Grasberg, Indonesia; Miller, 2014). Waste characterisation and management can be used to mitigate against the environmentally detrimental effects of PAF materials (e.g., AMD) and materials with a high ANC (alkaline mine drainage; Gomes et al., 2016). Consequently, the routine integration of mineralogical evaluations can improve static geochemical testing by guiding sample selection through mineralogical domaining of drill core and leading to advanced mineralogical and chemical characterisation techniques (Parbhakar-Fox et al., 2011).

7.3. Advanced core scanning technologies

Spectral imaging techniques including Corescan™ and SPECIM/TerraCore are becoming increasingly available for spectral mapping of drill core to provide integrated textural and mineralogical data. The smaller analytical area of imaging spectrometers (0.5 mm pixels) compared to the HyLogger-3 (equivalent 8 mm pixels) may reduce spectral interference from coexisting minerals in coarse grained rocks and allow more accurate mineral identification. Whilst VNIR-SWIR imaging is most widely available, thermal infrared (TIR) imaging has the capability to identify diverse carbonate-group minerals and map their textural relationships in drill core. Current limitations of TIR spectral cameras include the maximum attainable spectral range (up to 12,300 nm) which omits one of the diagnostic carbonate features (13,900 nm) used for carbonate diagnosis in this study. Future integration of other analytical techniques into core scanning platforms (e.g., micro XRF) have the potential to assist with identification and quantification of sulfide minerals (e.g., pyrite, chalcopyrite) and may allow determination of net acid producing potential proxies and routine textural assessments for acid rock drainage risk prediction (e.g., Parbhakar-Fox et al., 2011).

8. Conclusions

Integrated core scanning platforms that utilise both VNIR-SWIR and TIR spectral analysis provide the most complete tools for mineralogical domaining in drill core. Carbonate-group mineral speciation is most accurately resolved using TIR spectra which provide three diagnostic spectral features to resolve compositional solid solutions between in the Ca-Mg-Fe-Mn system. For geoenvironmental domaining, understanding the distribution of rapid acid neutralisers (calcite, ankerite) relative to siderite which has a negligible acid neutralising capacity is significant for sampling for more strategic static test and for long-term waste management plans. Identification of other mineral groups particularly sulfates also has implications for improving sampling for geoenvironmental test work and for more robust risk characterisation. As spectral imaging techniques become more widely available and provide the opportunity to map both mineralogy and texture in drill core, TIR imaging options will provide the most robust opportunity for quantitative carbonate mineral domaining in drill core. Adoption of geoenvironmental domaining during routine drill core scanning will allow potential environmental risks to be identified at the earliest life-of-mine stages.

Acknowledgments

The authors would like to acknowledge the support of CRC ORE (Project 20090048-10-P1B), established and supported by the Australian Government's Cooperative Research Centres Programme. We are grateful to David Green and Peter Harding of Mineral Resources Tasmania for assistance with the HyLogger at MRT. The MRT HyLogging node is part of the Australian Government funded National Virtual Core Library (NVCL) national infrastructure managed by AuScope Pty Ltd. We thank Copper Mines of Tasmania (CMT) and Vedanta Resources Plc for permission to use the Glen Lyell drill hole and providing associated data for this study. We would like to acknowledge two anonymous reviewers who have contributed to improve the manuscript. JM publishes with the permission of the Director of Mines, Mineral Resources Tasmania. Hylogger, HyLogging and TSG are registered Trademarks of CSIRO.

References

Berger, B.R., Ayuso, R.A., Wynn, J.C., Seal, R.R., 2008. Preliminary Model of Porphyry Copper Deposits: U.S. Geological Survey Open-File Report 2008–1321, p. 55.

Borden, R.K., 2003. Environmental geochemistry of the Bingham Canyon porphyry copper deposit, Utah. Environ. Geol. 43, 752–758.

Brough, C., Warrender, R., Bowell, R.J., Barnes, A., Parbhakar-Fox, A., 2013. The process mineralogy of mine wastes. Miner. Eng. 52, 125–135.

Corbett, K.D., Quilty, P.G., Calver, C.R., 2014. Geological Evolution of Tasmania. Geological Society of Australia, Tasmania Division.

Cudahy, T., Hewson, R., Caccetta, M., Roache, M., Whitbourn, L., Connor, P., Coward, D., Mason, P., Yang, K., Huntington, J., Quigley, M., 2009. Drill core logging of plagioclase feldspar composition and other minerals associated with Archean gold mineralization at Kambalda, Western Australia, using bidirectional thermal infrared reflectance system. Rev. Econ. Geol. 16, 223–235.

Dold, B., 2010. Basic concepts in environmental geochemistry of sulphide mine waste management. In: Kumar, Sunil (Ed.), Waste Management. INTECH Open Access Publications, pp. 173–198 (ISBN 978-953-7619-84-8).

Dold, B., 2017. Acid rock drainage prediction: a critical review. J. Geochem. Explor. 172, 120–132.

Downing, B.W., Giroux, G., 1993. Estimation of a waste rock ARD block model for the Windy Craggy massive sulphide deposit, northwestern British Columbia. Explor. Min. Geol. 2, 203–215.

Evangelou, V.P., Zhang, Y.L., 1995. A review: pyrite oxidation mechanisms and acid mine drainage prevention. Crit. Rev. Environ. Sci. Technol. 25, 141–199.

Gaffey, S., 1986. Spectral reflectance of carbonate minerals in the visible and near infrared (0.35–2.55 microns): calcite, aragonite and dolomite. Am. Mineral. 71, 151–162.

Gard Guide, 2014, <http://www.gardguide.com/index.php?title=Main_Page> (accessed 25 May 2016).

Gomes, H.I., Mayes, W.M., Rogerson, M., Stewart, D.I., Burke, I.T., 2016. Review: alkaline residues and the environment: a review of impacts, management practices and opportunities. J. Clean. Prod. 112 (Part 4), 3571–3582.

Green, D., Schodlok, M., in press. Characterisation of carbonate minerals from hyperspectral TIR scanning using features at 14 000 nm and 11 300 nm. Aust. J. Earth Sci., 7 http://dx.doi.org/10.1080/08120099.2016.1225601 (in press).

Holliday, J.R., Cooke, D.R., 2007. Advances in geological models and exploration methods for copper-gold porphyry deposits. In: Proceedings of the Decennial International Conference on Mineral Exploration 5, Toronto, Canada, pp. 791–809.

Huang, C.K., Kerr, P.F., 1960. Infrared study of the carbonate minerals. Am. Mineral. 45, 311–324.

Hunt, G.R., Salisbury, J.W., 1971. Visible and near-infrared spectra of minerals and rocks; II, Carbonates. Modern Geol. 2, 23–30.

Hunt, G.R., Salisbury, J.W., 1973. Visible and near infrared spectra of minerals and rocks; VI, additional silicates. Modern Geol. 4, 85–106.

Huntington, J., Whitbourn, L., Laukamp, C., Schodlok, M., Yang, K., Haest, M., Quigley, M., Mason, P., Berman, M., Green, A., 2011. Probing Australia's Subsurface with New 1, 2 and 3D Hyperspectral Logging Technologies for ''Whole-of-Mine-Life" Mineralogical Characterisation, Exploration Technologies 2011, pp. 40–47.

Huntington, J., Whitbourn, L., Mason, P., Schlodlok, M., Berman, M., 2010. HyLogging – Voluminous Industrial-scale Reflectance Spectroscopy of the Earth's Subsurface. Proceedings of ASD and IEEE GRS; Art, Science and Applications of Reflectance Spectroscopy Symposium, Boulder, CO, vol. II, p. 14.

Huston, D.L., Kamprad, J., 2001. Zonation of alteration facies at Western Tharsis: Implications for the genesis of Cu-Au deposits, Mount Lyell Field, Western Tasmania. Econ. Geol. 96, 1123–1132.

Imperial Metals, 2014, Annual Report <www.imperialmetals.com>.

Jambor, J.L., Dutrizac, J.E., Raudsepp, M., 2007. Measured and computed neutralization potentials from static tests of diverse rock types. Environ. Geol. 52, 1019–1031.

Jennings, K., Schodde, R., 2016, From mineral discovery to project delivery, SEG Newsletter, April 2006, No. 105.

John, D.A., Ayuso, R.A., Barton, M.D., Blakely, R.J., Bodnar, R.J., Dilles, J.H., Gray, F., Graybeal, F.T., Mars, J.C., McPhee, D.K., Seal, R.R., Taylor, R.D., Vikre, P.G., 2010, Porphyry copper deposit model, chap. B of Mineral deposit models for resource assessment: U.S. Geological Survey Scientific Investigations Report 2010-5070-B, 169 p.

Laakso, K., Peter, J.M., Rivard, B., White, H.P., 2016. Short-wave infrared spectral and geochemical characteristics of hydrothermal alteration at the Archean Izok Lake Zn-Cu-Pb-Ag volcanogenic massive sulfide deposit, Nunavut, Canada: application in exploration target vectoring. Econ. Geol. 111, 1223–1239.

Lapakko, K.A., 2002. Metal mine rock and waste characterisation tools: An overview. Posted on the Acid Rock Drainage Technology Initiative – Metal Mining Sector web page: <www.mackay.unr.edu.edu/adti>.

Lane, M.D., Christensen, P.R., 1997. Thermal infrared emission spectroscopy of anhydrous carbonates. J. Geophys. Res. 102, p. 25,581–25, 592.

Lang, J.R., Stanley, C.R., Thompson, J.F.H., Dunne, K.P.E., 1995. Na-K-Ca magmatichydrothermal alteration in alkalic porphyry Cu-Au deposits, British Columbia. Magmas, Fluids Ore Deposits 23, 339–366.

Large, R.R., 1992. Australian volcanic-hosted massive sulfide deposits: features, style, and genetic models. Econ. Geol. 87, 471–510.

Large, R.R., McPhie, J., Gemmell, J.B., Herrmann, W., Davidson, G.J., 2001. The Spectrum of ore deposit types, volcanic environments, alteration halos and related exploration vectors in submarine volcanic successions: Some Examples from Australia. Econ. Geol. 96, 1037–1054.

Laukamp, C., Cudahy, T., Thomas, M., Jones, M., Cleverley, J., Oliver, N., 2011. Hydrothermal mineral alteration patterns in the Mount Isa Inlier revealed by airborne hyperspectral data.-. Aust. J. Earth Sci. 58 (8), 917–936.

Logan, J.M., Mihalynuk, M.G., 2005, Regional geology and setting of the Cariboo, Bell, Springer and Northeast porphyry Cu-Au zones at Mount Polley, south-central British Columbia: BC Ministry of Energy and Mines, Geological Fieldwork 2004, Paper 2005-1, pp. 249–270.

Martini, B., 2013. Corescan: driving resource exploration and development with hyperspectral technology. GRSG Newsletter (67), 30–34.

Mason, P. Huntington, J.F., 2012, Hylogger 3 components and pre-processing: An overview. Northern Territory Geological Survey, Technical Note, 2012-002. p. 11.

Miller, S., 2014. Leading practice solutions for acid rock drainage prevention and control: a key to achieving a sustainable future for mineral resource development. In: Miller, H., Preuss, L. (Eds.), Proceedings of the Eighth Australian Workshop on Acid and Metalliferous Drainage, pp. 51–66.

Ong, C., Cudahy, T.J., 2014. Mapping contaminated soils: using remotely-sensed hyperspectral data to predict pH. Eur. J. Soil Sci. 65, 897–906.

Parbhakar-Fox, A., Lottermoser, B.L., 2015. A critical review of acid rock drainage prediction methods and practices. Miner. Eng. 82, 107–124.

Parbhakar-Fox, A., Edraki, M., Walters, S., Bradshaw, D., 2011. Development of a textural index for the prediction of acid rock drainage. Miner. Eng. 24, 1277–1287.

Parbhakar-Fox, A., Lottermoser, B.L., Bradshaw, D., 2013. Evaluating waste rock mineralogy and microtexture during kinetic testing for improved acid rock drainage prediction. Miner. Eng. 52, 111–124.

Pass, H.E., Cooke, D.R., Davidson, G., Maas, R., Dipple, G., Rees, C., Ferreira, L., Taylor, C., Deyell, C.L., 2014. Isotope geochemistry of the northeast zone, Mount Polley alkalic Cu-Au-Ag porphyry deposit, British Columbia: a case for carbonate assimilation. Econ. Geol. 109, 859–890.

Plumlee, G.S., 1999. The environmental geology of mineral deposits. In: Plumlee, G. S., Lodgson, M.J. (Eds.), The Environmental Geochemistry of Mineral Deposits Part A: Processes, Techniques and Health Issues, Reviews in Economic Geology, vol. 6B. Society of Economic Geologists, United States, Littleton, CO, pp. 71–116.

Reig, F.B., Adelanto, J.V.G., Moya Morenco, M.C.M., 2002. FTIR quantitative analysis of calcium carbonate (calcite) and silica (quartz) mixtures using the constant ratio method. Application to geological samples. Talanta 58, 811–821.

Seal II, R.R., Hammarstrom, J.M., 2003. Geoenvironmental models of mineral deposits: examples from massive sulfide and gold deposits: environmental Aspects of Mine Wastes. In: Jambor, J.L., Blowes, D.W., Ritchie, A.I.M. (Eds.), Mineralogical Association of Canada Short Series, vol. 31, pp. 11–50.

Schodlok, M.C., Whitbourn, L., Huntington, J., Mason, P., Green, A., Berman, A., Coward, D., Connor, P., Wright, W., Jolivet, M., Martinez, R., in press. HyLogger-3, a visible to shortwave and thermal infrared reflectance spectrometer system for drill core logging: functional description. Aust. J. Earth Sci., 12 http://dx.doi.org/10.1080/08120099.2016.1231133 (in press).

Seedorff, E., Dilles, J.H., Proffett, J.M., Jr., Einaudi, M.T., Zurcher, L., Stavast, W.J.A., Johnson, D.A., Barton, M.D., 2005, Porphyry deposits: Characteristics and origin of hypogene features: Economic Geology 100th Anniversary Volume, pp. 251–298.

Sillitoe, R.H., 2010. Porphyry copper systems. Econ. Geol. 105, 3–41.

Smart, R., Skinner, W.M., Levay, G., Gerson, A.R., Thomas, J.E., Sobieraj, H., Schumann, R., Weisener, C.G., Weber, P.A., Miller, S.D., Stewart, W.A., 2002. ARD Test Handbook: Project P387, A Prediction and Kinetic Control of Acid Mine Drainage. AMIRA, International Ltd., Melbourne, Australia, p. 42.

Taylor, C.D., Zierenberg, R.A., Goldfarb, R.J., Kilburn, J.E., Seal II, R.R., Kleinkopf, M.D., 1995. Volcanic-Associated Massive Sulfide Deposits (Models 24a-b, 28a; Singer 1986a, b; Cox, 1986). In: Preliminary Compilation of Descriptive Geoenvironmental Mineral Deposit Models. U.S Geological Survey Open-File Report 90-831, pp. 137–144.

van Ruitenbeek, F.J.A., Cudahy, T., van der Meer, F.D., Hale, M., 2012. Characterization of the hydrothermal systems associated with Archean VMS-mineralization at Panorama, Western Australia, using hyperspectral, geochemical and goethermometric data. Ore Geol. Rev. 45, 33–46.

Walshe, J.L., Solomon, M., 1981. An investigation into the environment of formation of the volcanic-hosted Mt. Lyell copper deposits using geology, mineralogy, stable isotopes, and a six-component chlorite solid solution model. Econ. Geol. 76, 246–284.

Weber, P.A., Thomas, J.E., Skinner, W.M., Smart, R., St, C., 2005. A method to determine the acid neutralisation capacity of rock samples. Can. Mineral. 43, 1183–1192.

White, W.W., Lapakko, K.A., Cox, R.L., 1999. Static test methods most commonly used to predict acid mine drainage: practical guidelines for use and interpretation. In: Plumlee, G.S., Lodgson, M.J. (Eds.), The Environmental Geochemistry of Mineral Deposits Part A: Processes, Techniques, and Health Issues, Reviews of Economic Geology, vol.6A, pp. 325–338.

Yang, K., Huntington, J.F., Gemmell, J.B., Scott, K.M., 2011. Variations in composition and abundance of white mica in the hydrothermal alteration system at Hellyer, Tasmania, as revealed by infrared reflectance spectroscopy. J. Geochem. Explor. 108, 143–156.

Fig. 1. (A) Short wave infrared (SWIR) reflectance spectra for reference library samples of carbonate and chlorite minerals showing the position of key diagnostic features and potential interferences with chlorite minerals. (B) Long wave infrared (LWIR or TIR) reflectance spectra for carbonate-group minerals and the positions of key spectral features used for diagnosis. Reflectance spectra of pure minerals from the TSG reference library.

Fig. 2. Geological map of the Mount Lyell VHMS field, located in western Tasmania, Australia. The location of drill hole GLD001 used in this study is indicated by the red star. Modified from Corbett et al. (2014).

Fig. 3. The location of the Mount Polley porphyry Cu-Au deposit, British Columbia, Canada and alteration map and cross section showing the location of the drill hole studied (WB04-26) on Section 18. Modified from Pass et al. (2014).

Fig. 4. Drill core samples from Mount Lyell mineral field. (A) Carbonate veins cross cutting schist, Domain 1, 131.3 m depth; (B) Irregular carbonate veins, Domain 3, 565.8 m depth; (C) Fine grained chloritic schist with no significant carbonate veining, Domain 4, 750.0 m depth; (D) Carbonate-rich breccia, Domain 5, 900.0 m.

Fig. 5. Drill core samples from Mount Polley, Northeast Zone. (A) Brecciated porphyritic monzonite cemented by white calcite, 68.1 m depth; (B) Nicola Group basalt with vein breccia and infill cement, interpreted to be calcite by field tests.

Fig. 6. Discrimination diagrams for diagnostic spectral features for carbonate minerals with end member carbonate fields from Green and Schodlok (in press). (A) Carbonate 13,900 vs 11,300 nm spectral features and mineral classification for Glen Lyell samples; (B) Carbonate 11,300 vs. 6500 nm spectral features and mineral classification for Glen Lyell samples. (C) Carbonate 13,900 vs 11,300 nm spectral features of calcite from Mount Polley samples. (D) 11,300 vs. 6500 nm discrimination diagram for Mount Polley calcite with classifications according to high spectral certainty (Calcite High) and moderate certainty (Calcite Mod.) after filtering.

Fig. 7. Downhole logs including whole rock assays, spectral data (counts), XRPD mineralogy and acid base accounting for Glen Lyell drill hole GLD001 highlighting five carbonate domains (D1 to D5) and two host rock domains (HR) which were sampled. Abbreviations: NAPP, net acid producing potential; NAF, non-acid forming; PAF, potentially acid forming.

Fig. 8. Downhole logs showing calcite distribution (counts), XRPD mineralogy and acid base accounting for Mount Polley drill hole WB04-26. Abbreviations: NAPP, net acid producing potential; NAF, non-acid forming; PAF, potentially acid forming.

Fig. 9. Electron microprobe analyses (EMPA) analyses from the studied samples. (A) Molar CaCO3-MgCO3-FeCO3 ternary diagram; (B) Molar CaCO3-MnCO3-FeCO3 ternary diagram. (C) Binary molar MnCO3-CaCO3 diagram; (D) Molar MnCO3-FeCO3 diagram.

Fig. 10. Classification plots for geoenvironmental risk classification from Glen Lyell drill hole GLD001 and from Mount Polley drill hole WB04-26. (A) Net acid producing potential (NAPP) vs. NAG pH classification diagram; (B) Paste pH vs. NAG pH classification diagram (after Weber et al., 2005).

Table 1. Positions of key SWIR and TIR spectral features for selected carbonate-group minerals. Positions measured from reflectance spectra of pure minerals in The Spectral Geologist (TSG) reference library and from Green and Schodlok (in press). Neutralising potential (NP) values for each carbonate mineral are also shown from Jambor et al. (2007).

Table 2. Quantitative mineralogy (by XRPD), total C and S, and acid base accounting calculations for carbonate bearing domains 1–5 and host rock domains for Glen Lyell drill hole GLD001.

Table 3. Quantitative mineralogy (by XRPD), total C and S, and acid base accounting calculations for Mount Polley drill hole WB04-26.

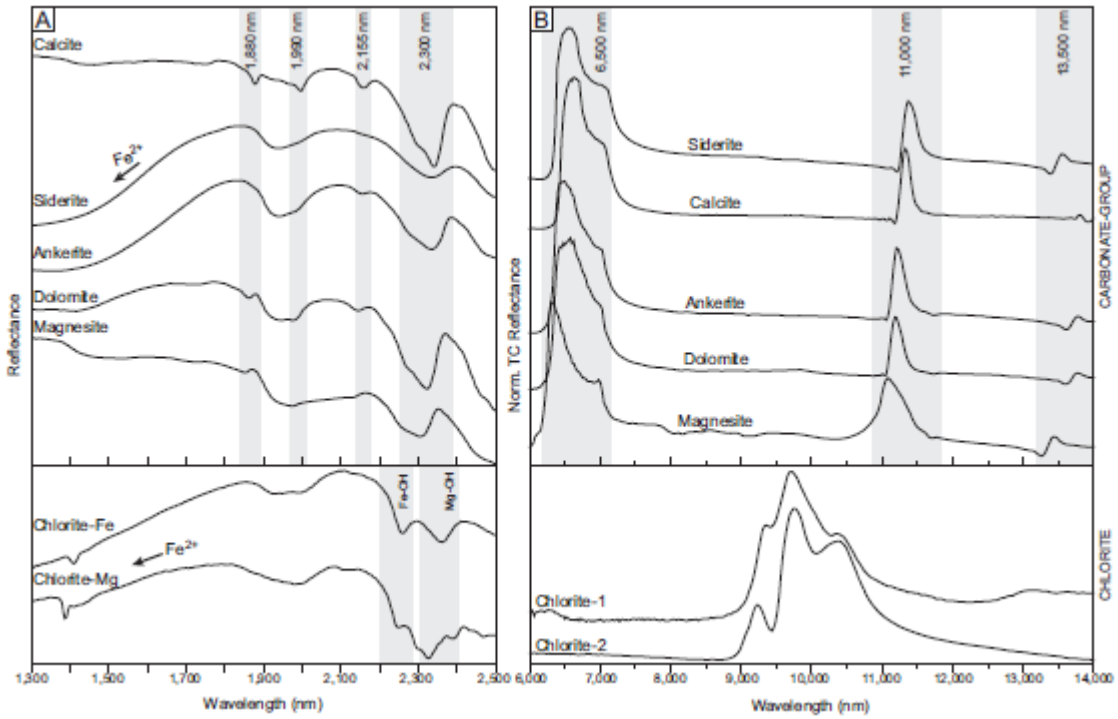
A
Calcite
1,880 nm
1,990 nm
2,155 nm
2,300 nm
Fe2+
Siderite
Ankerite
Dolomite
Magnesite
Reflectance
Fe-OH
Mg-OH
Chlorite-Fe
Fe2+
Chlorite-Mg
1,300
1,500
1,700
1,900
2,100
2,300
2,500
Wavelength (nm)
B
6,500 nm
11,000 nm
13,500 nm
Norm. TC Reflectance
Siderite
Calcite
Ankerite
Dolomite
Magnesite
CARBONATE-GROUP
Chlorite-1
Chlorite-2
CHLORITE
6,000
7,000
8,000
9,000
10,000
11,000
12,000
13,000
14,000
Wavelength (nm)

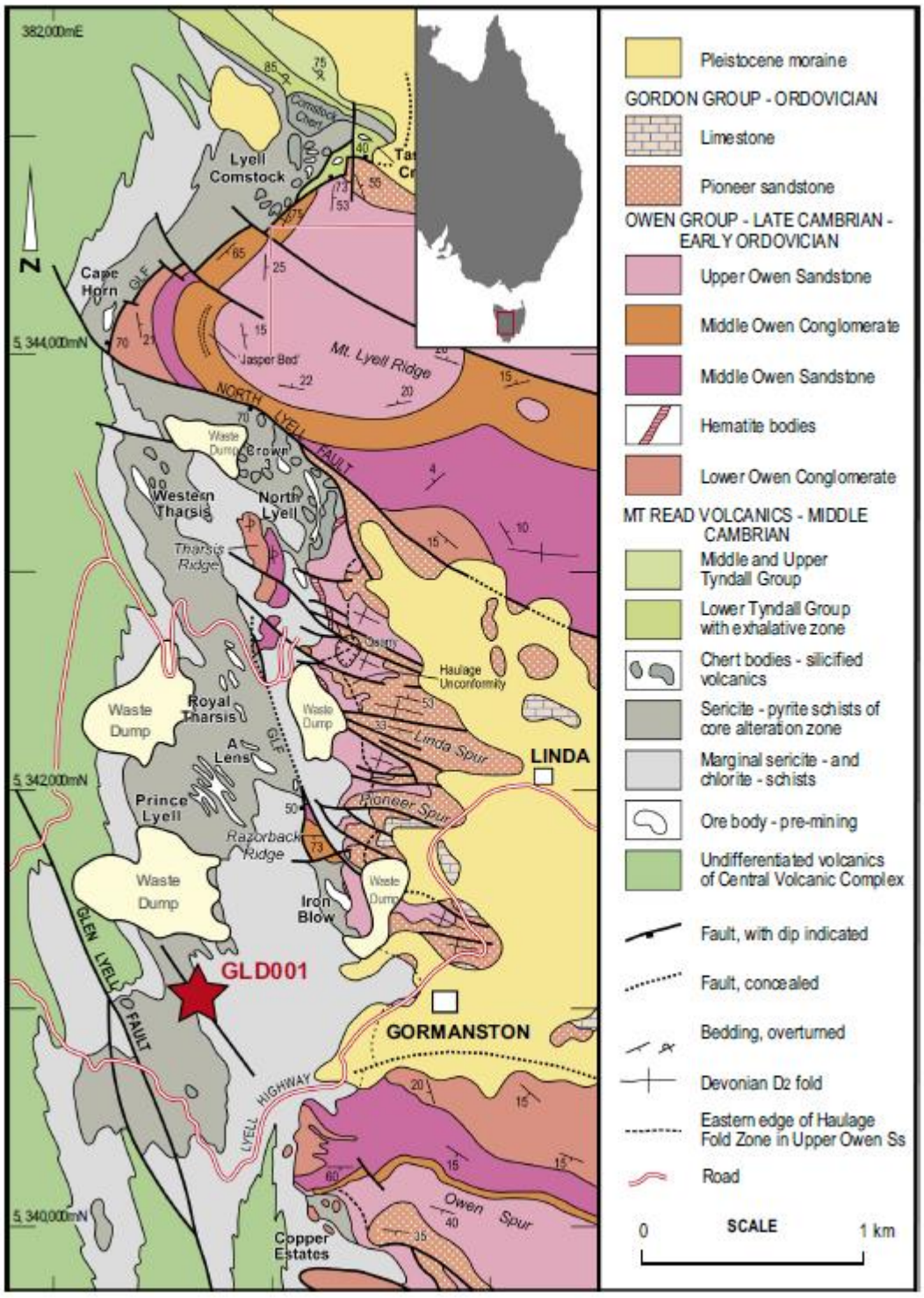
382,000mE
5,344,000mN
5,342,000mN
5,340,000mN
N
Lyell Comstock
Comstock Chert
Cape Horn
GLF
Jasper Bed
Mt. Lyell Ridge
NORTH LYELL FAULT
Waste Dump
Brown
Western Tharsis
North Lyell
Tharsis Ridge
Haulage Unconformity
Waste Dump
Royal Tharsis
A Lens
Linda Spur
LINDA
Prince Lyell
Pioneer Spur
Razorback Ridge
Waste Dump
Iron Blow
Waste Dump
GLD001
GLEN LYELL FAULT
GORMANSTON
LYELL HIGHWAY
Owen Spur
Copper Estates
Pleistocene moraine
GORDON GROUP - ORDOVICIAN
Limestone
Pioneer sandstone
OWEN GROUP - LATE CAMBRIAN - EARLY ORDOVICIAN
Upper Owen Sandstone
Middle Owen Conglomerate
Middle Owen Sandstone
Hematite bodies
Lower Owen Conglomerate
MT READ VOLCANICS - MIDDLE CAMBRIAN
Middle and Upper Tyndall Group
Lower Tyndall Group with exhalative zone
Chert bodies - silicified volcanics
Sericite - pyrite schists of core alteration zone
Marginal sericite - and chlorite - schists
Ore body - pre-mining
Undifferentiated volcanics of Central Volcanic Complex
Fault, with dip indicated
Fault, concealed
Bedding, overturned
Devonian D2 fold
Eastern edge of Haulage Fold Zone in Upper Owen Ss
Road
0
SCALE
1 km

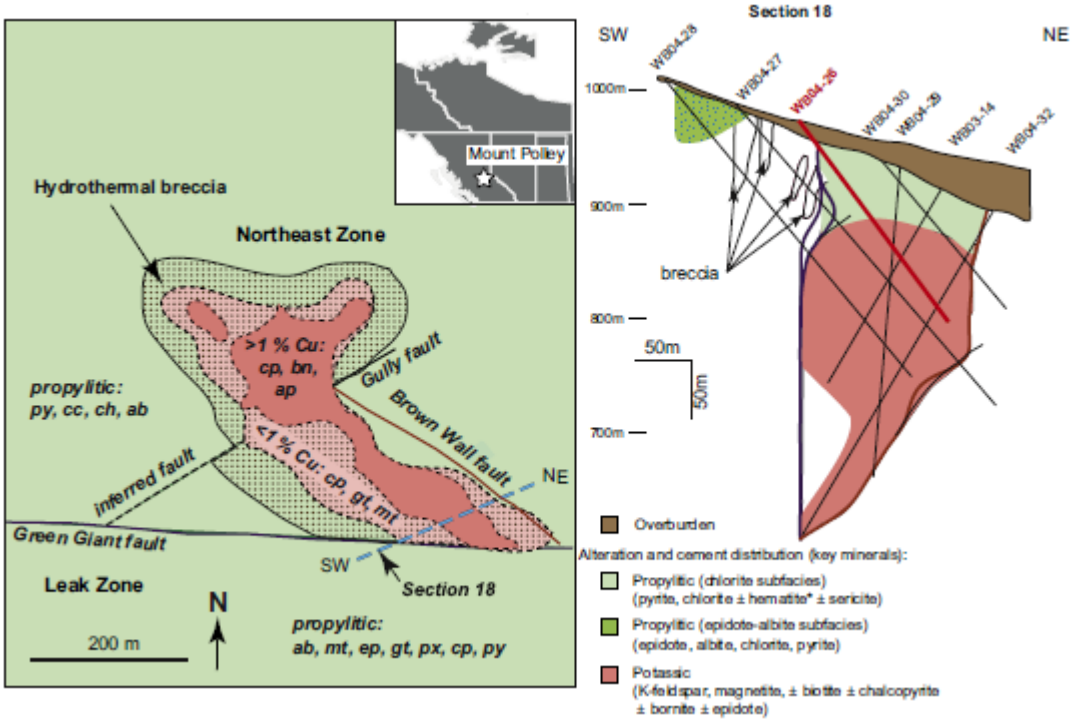
Mount Polley
Hydrothermal breccia
Northeast Zone
>1 % Cu:
cp, bn,
ap
propylitic:
py, cc, ch, ab
Gully fault
Brown Wall fault
inferred fault
<1 % Cu: cp, gt, mt
Green Giant fault
NE
SW
Section 18
Leak Zone
N
200 m
propylitic:
ab, mt, ep, gt, px, cp, py
Section 18
SW
NE
WB04-28
WB04-27
WB04-26
WB04-30
WB04-29
WB03-14
WB04-32
1000m
900m
800m
700m
breccia
50m
50m
Overburden
Alteration and cement distribution (key minerals):
Propylitic (chlorite subfacies)
(pyrite, chlorite ± hematite* ± sericite)
Propylitic (epidote-albite subfacies)
(epidote, albite, chlorite, pyrite)
Potassic
(K-feldspar, magnetite, ± biotite ± chalcopyrite
± bornite ± epidote)

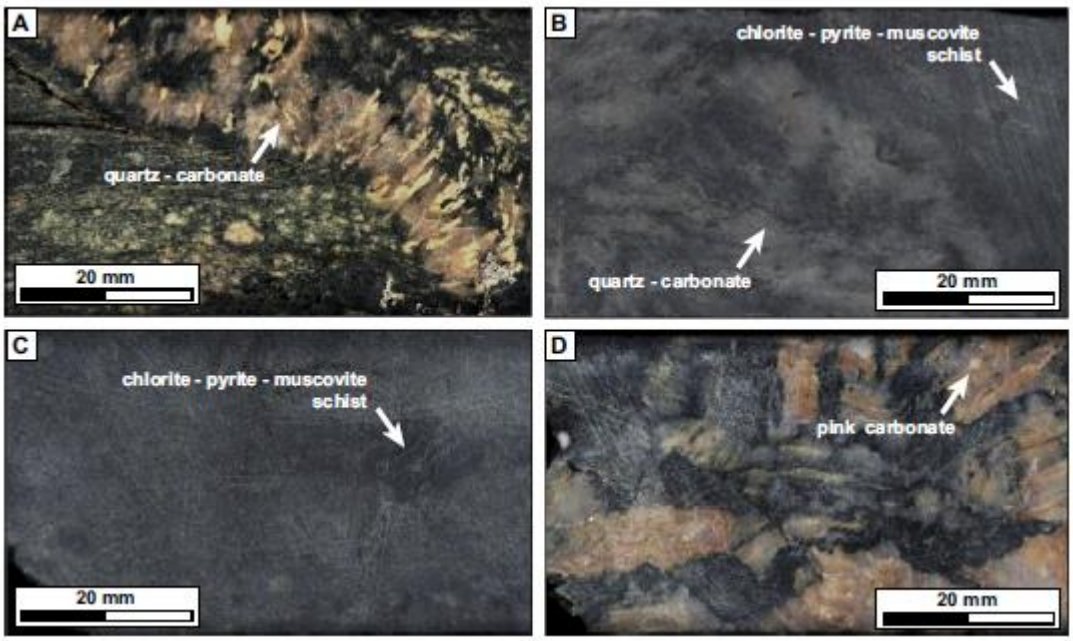
A
quartz - carbonate
20 mm
B
chlorite - pyrite - muscovite schist
quartz - carbonate
20 mm
C
chlorite - pyrite - muscovite schist
20 mm
D
pink carbonate
20 mm

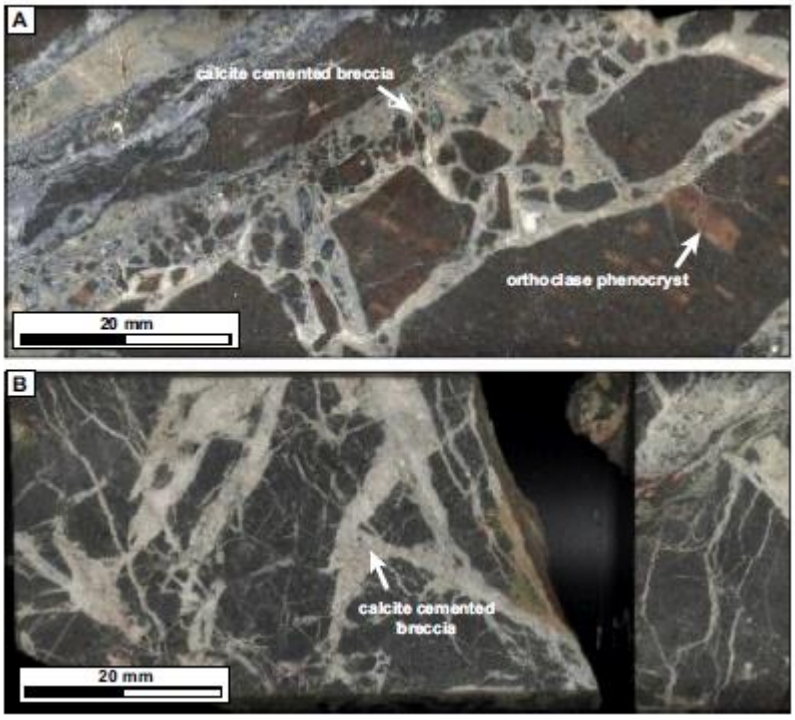
A
calcite cemented breccia
orthoclase phenocryst
20 mm
B
calcite cemented
breccia
20 mm

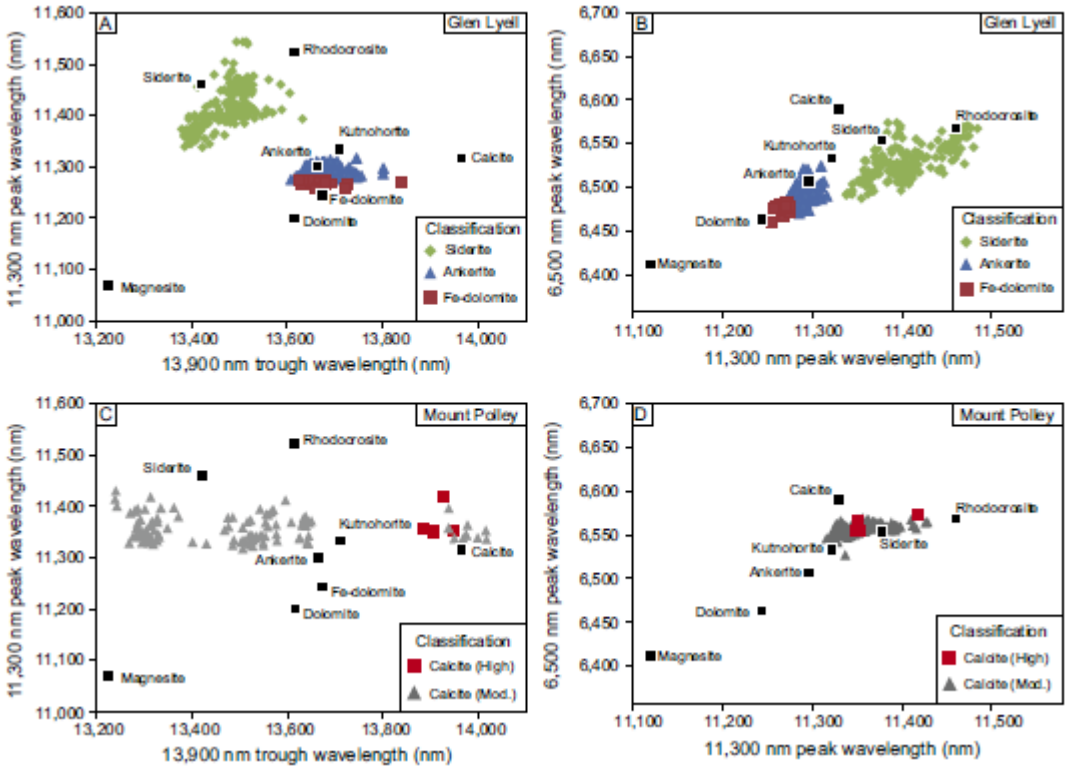
A
Glen Lyell
Rhodocrosite
Siderite
Kutnohorite
Ankerite
Calcite
Fe-dolomite
Dolomite
Magnesite
Classification
Siderite
Ankerite
Fe-dolomite
11,300 nm peak wavelength (nm)
13,900 nm trough wavelength (nm)
B
Glen Lyell
Calcite
Siderite
Rhodocrosite
Kutnohorite
Ankerite
Dolomite
Magnesite
Classification
Siderite
Ankerite
Fe-dolomite
6,500 nm peak wavelength (nm)
11,300 nm peak wavelength (nm)
C
Mount Polley
Rhodocrosite
Siderite
Kutnohorite
Calcite
Ankerite
Fe-dolomite
Dolomite
Magnesite
Classification
Calcite (High)
Calcite (Mod.)
11,300 nm peak wavelength (nm)
13,900 nm trough wavelength (nm)
D
Mount Polley
Calcite
Rhodocrosite
Kutnohorite
Siderite
Ankerite
Dolomite
Magnesite
Classification
Calcite (High)
Calcite (Mod.)
6,500 nm peak wavelength (nm)
11,300 nm peak wavelength (nm)

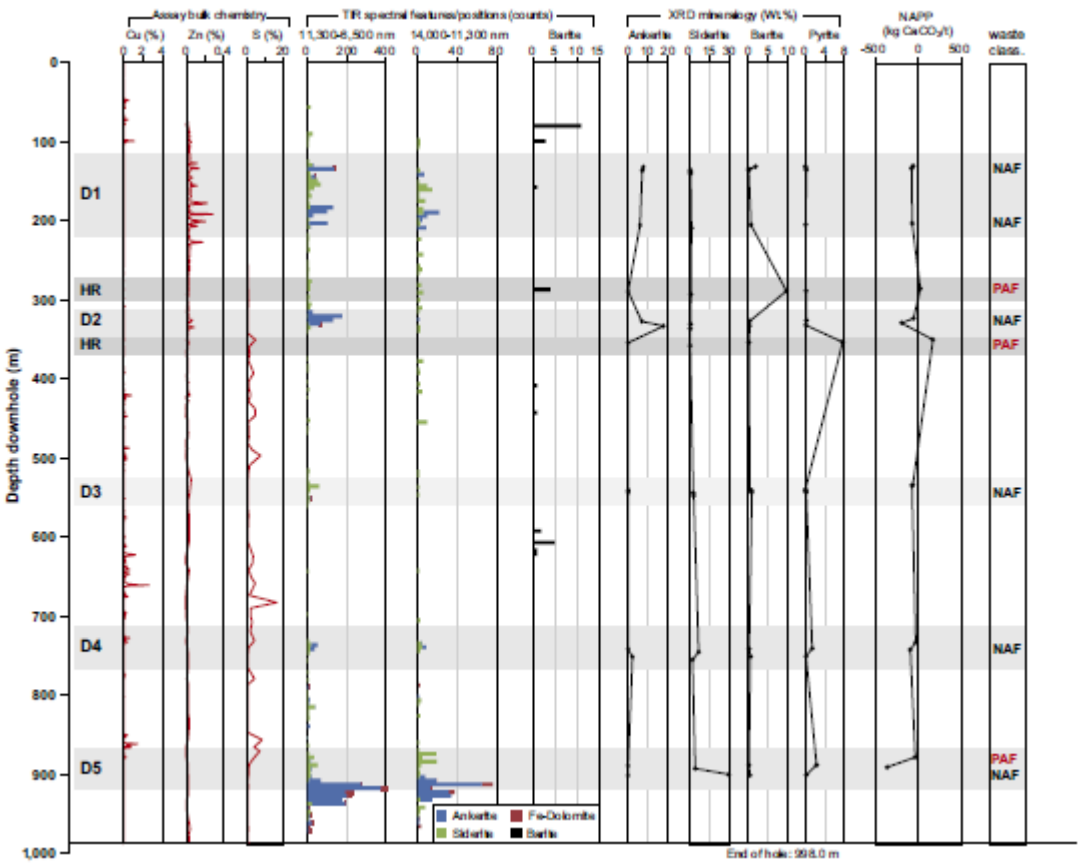
Assay bulk chemistry
Cu (%)
Zn (%)
S (%)
TIR spectral features/positions (counts)
11,300-8,500 nm
14,000-11,200 nm
Barite
XRD mineralogy (Wt.%)
Ankerite
Siderite
Barite
Pyrite
NAPP (kg CaCO3/t)
waste class
Depth downhole (m)
D1
HR
D2
HR
D3
D4
D5
NAF
PAF
Ankerite
Fe-Dolomite
Siderite
Barite
End of hole: 998.0 m

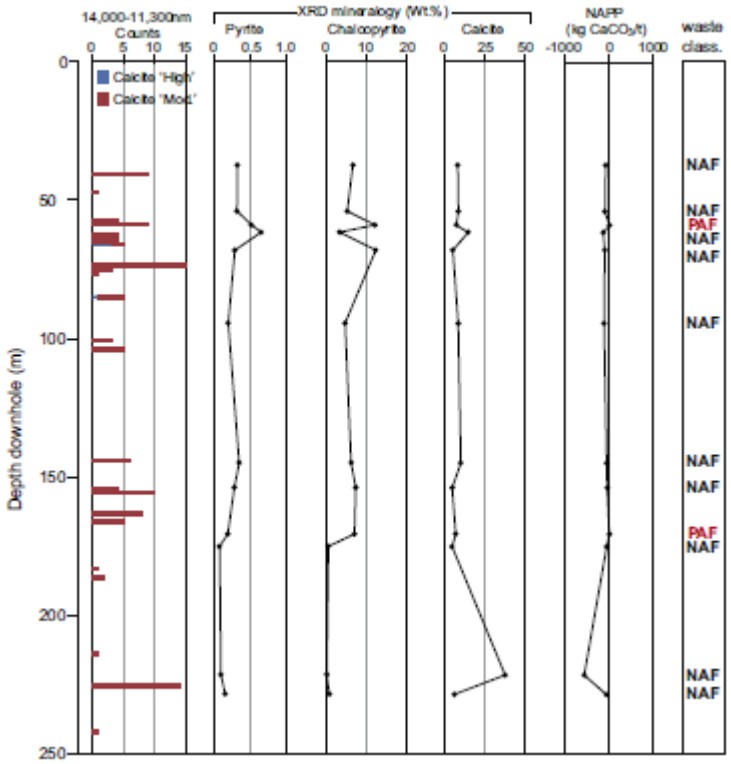
14,000-11,300nm
Counts
0 5 10 15
Calcite 'High'
Calcite 'Mod'
XRD mineralogy (Wt.%)
Pyrite
0 0.5 1.0
Chalcopyrite
0 10 20
Calcite
0 25 50
NAPP
(kg CaCO3/t)
-1000 0 1000
waste
class.
Depth downhole (m)
0
50
100
150
200
250
NAF
NAF
PAF
NAF
NAF
NAF
NAF
NAF
PAF
NAF
NAF
NAF

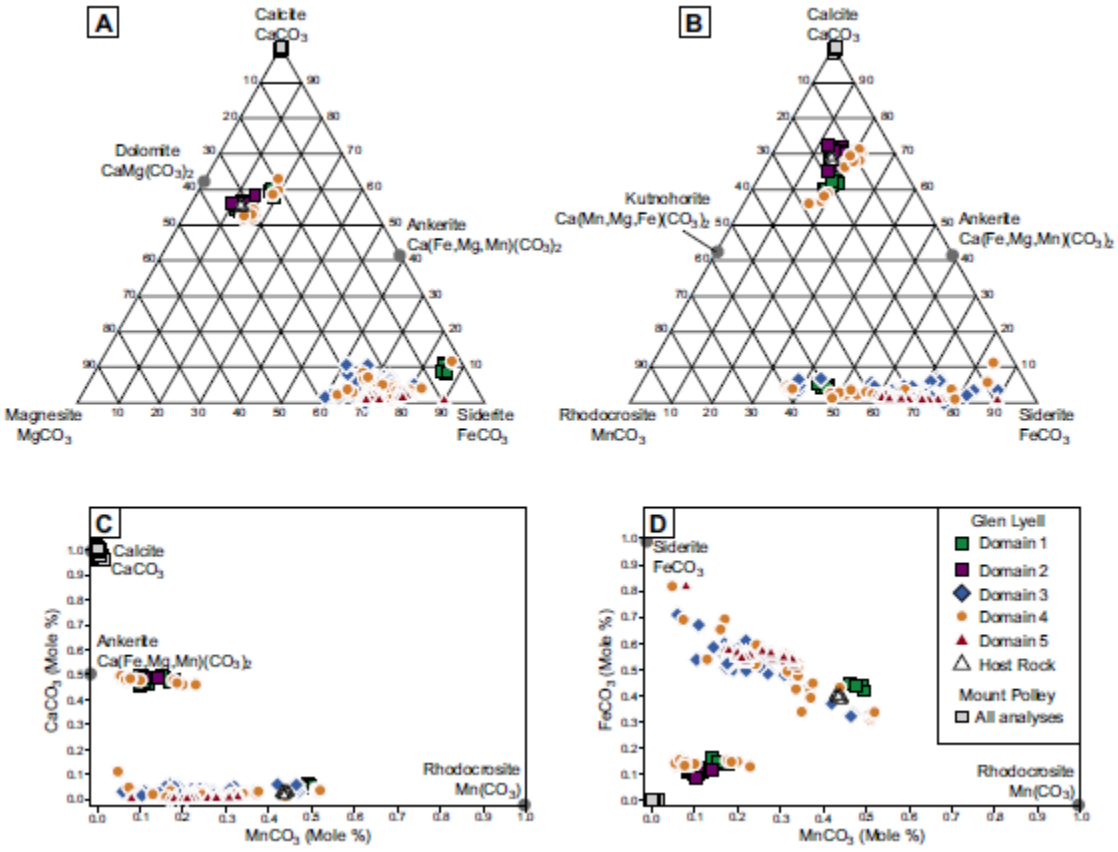
A
Calcite
CaCO3
Dolomite
CaMg(CO3)2
Ankerite
Ca(Fe,Mg,Mn)(CO3)2
Magnesite
MgCO3
Siderite
FeCO3
B
Calcite
CaCO3
Kutnohorite
Ca(Mn,Mg,Fe)(CO3)2
Ankerite
Ca(Fe,Mg,Mn)(CO3)2
Rhodocrosite
MnCO3
Siderite
FeCO3
C
Calcite
CaCO3
Ankerite
Ca(Fe,Mg,Mn)(CO3)2
Rhodocrosite
Mn(CO3)
CaCO3 (Mole %)
MnCO3 (Mole %)
D
Siderite
FeCO3
Rhodocrosite
Mn(CO3)
FeCO3 (Mole %)
MnCO3 (Mole %)
Glen Lyell
Domain 1
Domain 2
Domain 3
Domain 4
Domain 5
Host Rock
Mount Polley
All analyses

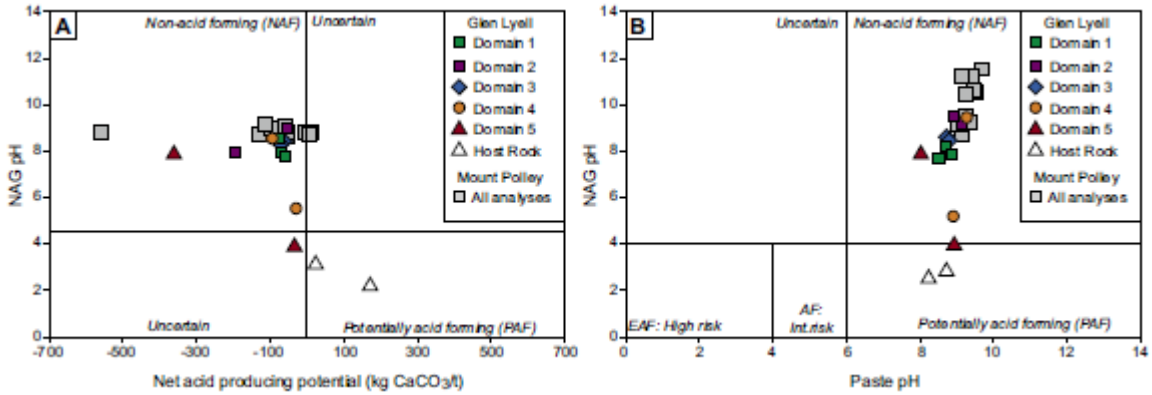
A
Non-acid forming (NAF)
Uncertain
Uncertain
Potentially acid forming (PAF)
Glen Lyell
Domain 1
Domain 2
Domain 3
Domain 4
Domain 5
Host Rock
Mount Polley
All analyses
NAG pH
Net acid producing potential (kg CaCO3/t)
B
Uncertain
Non-acid forming (NAF)
EAF: High risk
AF: Int.risk
Potentially acid forming (PAF)
Paste pH

Mineral	Formula	SWIR				TIR			NP
		1880 nm	1990 nm	2155 nm	2335 nm	6500 nm	11,300 nm	13,900 nm	kg $CaCO_3$/t
Rhodochrosite	$MnCO_3$				2,350–2355	6555	11,533	13,657	870
Calcite	$CaCO_3$	1880	1992	2156	2,350–2355	6583	11,325	13,950	1000
Ankerite	$Ca(Mg,Fe,Mn)(CO_3)_2$			2153	2,330–2340	6536	11,249	13,656	970
Siderite	$FeCO_3$		1990	2157	2,320–2350	6555	11,427	13,591	864
Dolomite	$CaMg(CO_3)_2$	1865	1940	2140	2,320–2328	6536	11,190	13,761	1086
Magnesite	$MgCO_3$	1850		2130	2302	6338	11,533	13,657	1187

	Glen Lyell drill hole GLD001 sample depth (m)											
	Domain 1			Host rock	Domain 2		Host rock	Domain 3		Domain 4		Domain 5	
Depth (m)	131.3	134.3	204.8	288.3	326.1	332.0	353.3	539.5	540.0	740.2	750.0	887.3	900.0
Quartz	60.4	50.5	52.1	61.9	42.1	60.0	54.4	67.3	47.0	69.7	51.8	54.0	66.9
Muscovite	22.7	37.0	35.1	16.3	42.0	12.7	13.4	21.4	44.2	19.3	39.0	31.6	0.4
Chlorite	4.2	1.9	3.0	10.8	6.1	3.9	23.4	8.9	4.6	0.1	4.1	9.0	0.0
Biotite	1.4	1.4	1.3	0.5	0.9	1.2	3.2	0.6	0.9	1.8	0.7	1.1	0.1
Ankerite	9.4	9.0	7.3	0.0	8.4	21.8	0.0	0.1	0.2	0.1	2.7	0.0	0.0
Siderite	0.0	0.1	0.6	0.3	0.1	0.0	0.0	1.5	2.2	7.9	1.2	2.6	32.0
Barite	1.8	0.0	0.6	10.1	0.2	0.3	0.0	0.3	0.8	0.1	0.4	0.0	0.3
Pyrite	0.0	0.1	0.0	0.1	0.2	0.1	5.6	0.0	0.1	1.0	0.1	1.7	0.1
Rwp	4.6	5.0	4.7	5.0	4.9	4.4	3.8	4.2	4.4	3.7	4.6	4.0	3.2
Rexp	13.3	12.6	11.6	13.0	14.1	11.3	11.6	11.4	12.5	13.0	13.2	10.5	6.9
GOF	9.3	8.8	8.2	8.6	9.8	7.6	7.4	7.5	8.6	8.4	9.0	6.9	4.7
Total C (wt.%)	0.85	0.96	0.88	0.31	0.70	2.73	0.16	0.82	0.95	0.74	1.16	0.94	4.37
Total S (wt.%)	0.36	0.10	0.13	1.57	0.12	1.09	5.92	0.12	0.21	1.02	0.11	1.42	0.10
Paste pH	8.5	8.7	8.9	8.6	8.8	9.0	8.2	8.7	8.7	8.6	8.9	8.5	8.0
NAG pH	7.8	8.6	7.9	3.2	9.0	7.9	2.3	8.4	8.3	5.5	8.5	4.0	8.0
Waste classification	NAF	NAF	NAF	PAF	NAF	NAF	PAF	NAF	NAF	NAF	NAF	PAF	NAF
NP (kg $CaCO_3$/t)	70.8	79.7	73.2	25.8	58.2	227.8	13.6	68.1	79.3	61.9	96.4	78.7	364.7
MPA (kg $CaCO_3$/t)	11.3	3.2	4.0	48.1	3.8	34.2	185.0	3.9	6.7	32.0	3.6	44.5	3.1
NAPP (kg $CaCO_3$/t)	−59.4	−76.4	−69.2	23.3	−54.4	−193.6	171.4	−64.3	−72.7	−29.9	−92.9	−34.3	−361.6
Waste Classification	NAF	NAF	NAF	PAF	NAF	NAF	PAF	NAF	NAF	NAF	NAF	NAF	NAF

Abbreviations: Rwp, weighted profile R-factor; Rexp, expected R-factor; GOF, goodness of fit; NAG, net acid generation; NP, neutralising potential; MPA, maximum potential acidity; NAPP, net acid producing potential; NAF, non-acid forming; PAF, potentially acid forming.

	Mount Polley drill hole WB04-26 sample depth (m)											
Depth (m)	37.3	54.0	59.0	61.6	68.1	94.5	145.0	153.9	170.7	175.2	221.6	228.6
Orthoclase	31.0	35.5	33.1	34.2	22.8	18.2	32.3	29.3	33.8	38.4	4.5	12.3
Anorthite	8.8	6.6	3.7	5.4	18.5	7.1	6.9	9.8	9.1	5.4	3.8	9.4
Albite	15.7	13.4	13.4	15.5	5.8	35.3	14.7	10.5	10.0	3.4	32.8	43.1
Hornblende	0.9	0.8	2.0	1.4	2.1	0.8	1.5	2.4	2.0	1.8	0.5	1.7
Muscovite	6.1	7.6	5.9	4.2	9.7	7.9	5.7	7.5	6.6	13.0	1.7	6.9
Biotite	2.9	3.4	2.5	3.6	2.3	2.7	4.1	3.2	4.4	7.2	1.1	4.7
Clinochlore	10.7	10.7	11.4	7.2	8.7	9.5	8.9	13.4	9.0	10.8	8.4	7.1
Epidote	1.1	0.6	1.4	1.0	1.2	0.5	1.9	2.3	2.6	2.3	0.6	0.9
Magnetite	3.9	4.7	3.7	4.1	3.3	2.9	5.2	6.8	4.5	6.3	1.7	4.0
Chalcopyrite	6.6	5.2	12.1	3.3	12.3	4.6	6.2	7.3	7.0	0.5	0.1	0.7
Pyrite	0.3	0.3	0.5	0.7	0.3	0.2	0.3	0.3	0.2	0.0	0.0	0.1
Calcite	8.1	8.6	7.3	14.7	5.1	8.4	10.1	4.7	6.9	4.6	37.7	6.0
Analcime	2.3	0.0	0.0	0.0	0.5	0.0	0.2	0.0	0.1	0.0	0.0	0.2
Quartz	0.8	2.3	1.1	3.9	7.0	1.1	1.1	0.5	1.8	4.1	6.4	1.3
Schorl	0.7	0.4	1.7	0.9	0.5	0.8	0.9	2.0	2.2	2.3	0.8	1.5
Rwp	8.9	8.7	9.9	10.2	14.1	9.1	8.9	9.4	11.0	12.1	10.0	10.2
Rexp	5.1	5.0	4.8	5.2	5.6	5.2	4.9	4.7	5.1	5.3	6.2	5.1
GOF	1.8	1.7	2.1	2.0	2.5	1.7	1.8	2.0	2.1	2.3	1.6	2.0
Total C (wt.%)	1.1	1.3	0.9	2.0	1.2	1.4	1.2	0.7	0.9	0.7	6.7	0.9
Total S (wt.%)	0.7	0.5	2.9	1.2	0.1	0.2	1.6	1.9	2.6	0.2	0.1	0.4
Paste pH	8.8	9.0	8.8	8.7	9.0	9.2	8.6	8.8	8.8	8.8	8.8	9.1
NAG pH	8.5	10.1	8.7	8.7	10.0	11.3	9.0	8.9	8.5	10.9	11.1	10.5
Risk classification	NAF	NAF	NAF	NAF	NAF	NAF	NAF	NAF	NAF	NAF	NAF	NAF
NP (kg $CaCO_3$/t)	95.4	106.4	78.1	167.2	101.5	117.5	101.8	61.4	73.4	62.1	561.1	71.6
MPA (kg $CaCO_3$/t)	22.1	14.1	91.1	37.9	4.5	4.9	49.0	58.4	80.3	6.9	3.6	11.6
NAPP (kg $CaCO_3$/t)	−73.3	−92.3	13.0	−129.3	−97.0	−112.7	−52.8	−3.0	6.9	−55.2	−557.5	−60.0
Risk classification	NAF	NAF	PAF	NAF	NAF	NAF	NAF	NAF	PAF	NAF	NAF	NAF

Abbreviations: Rwp, weighted profile R-factor; Rexp, expected R-factor; GOF, goodness of fit; NAG, net acid generation; NP, neutralising potential; MPA, maximum potential acidity; NAPP, net acid producing potential; NAF, non-acid forming; PAF, potentially acid forming.